Annu. Rev. Fluid Mech. 2002. 34:503–29

SYNTHETIC JETS

Ari Glezer[1] and Michael Amitay[2]
[1]*George W. Woodruff School of Mechanical Engineering, Georgia Institute of Technology, Atlanta, Georgia 30332-0405; e-mail: ari.glezer@me.gatech.edu*
[2]*Aerospace, Transportation, and Advanced Systems Laboratory, Georgia Technical Research Institute, Atlanta, Georgia 30332-0800; e-mail: michael.amitay@me.gatech.edu*

Dedicated to Professor D.E. Coles, who conceived synthetic shear flows.

Key Words synthetic jets, vortices, jet cross-flow interaction, turbulence, boundary-layer separation, aerodynamic forces

■ **Abstract** The evolution of a synthetic (zero-net mass flux) jet and the flow mechanisms of its interaction with a cross flow are reviewed. An isolated synthetic jet is produced by the interactions of a train of vortices that are typically formed by alternating momentary ejection and suction of fluid across an orifice such that the net mass flux is zero. A unique feature of these jets is that they are formed entirely from the working fluid of the flow system in which they are deployed and, thus, can transfer linear momentum to the flow system without net mass injection across the flow boundary. Synthetic jets can be produced over a broad range of length and timescale, and their unique attributes make them attractive fluidic actuators for a number of flow control applications. The interaction of synthetic jets with an external cross flow over the surface in which they are mounted can displace the local streamlines and induce an apparent or virtual change in the shape of the surface, thereby effecting flow changes on length scales that are one to two orders of magnitude larger than the characteristic scale of the jets. This control approach emphasizes an actuation frequency that is high enough so that the interaction domain between the actuator and the cross flow is virtually invariant on the global timescale of the flow, and therefore, global effects such as changes in aerodynamic forces are effectively decoupled from the operating frequency of the actuators.

1. OVERVIEW

Jet-like flows having complex spatial and temporal characteristics can be engendered in a quiescent medium (or in a cross flow) by the advection and interactions of trains of discrete vortical structures (e.g., Saffman 1981). The hydrodynamic impulse that is necessary to form each of these vortices is imparted at the flow boundary by the momentary discharge of slugs of fluid through an orifice. The flow typically separates at the edge of the orifice, and a vortex sheet is formed and rolls into an isolated vortex that is subsequently advected away under its own self-induced velocity. Depending on the flow symmetry and the repetition rate, the dynamics and interactions of the vortical structures within a pulsed jet can lead to

spatial evolution that is remarkably different from the evolution of a continuous (conventional) jet having the same orifice and time-averaged flux of streamwise momentum. Moreover, discrete vortical structures can also be formed within a continuous jet by deliberate temporal modulation of its streamwise momentum flux, which, depending on the degree and frequency of modulation, can lead to radical modification of the unmodulated jet. For example, Lee & Reynolds (1985) demonstrated that small changes in the azimuthal formation of successive vortex rings in a circular jet can alter their trajectories and result in spectacular far-field "bifurcation" or "blooming."

"Synthetic" jet flows are similar to pulsed jets in that they are also produced by the advection and interactions of trains of discrete vortical structures. However, a unique feature of synthetic jets is that they are formed entirely from the working fluid of the flow system in which they are deployed and, thus, can transfer linear momentum to the flow system without net mass injection across the flow boundary. The fluid that is necessary to synthesize the jet is typically supplied by intermittent suction through the same flow orifice between consecutive ejections. Because the characteristic dimensions of the ensuing jet scale with the orifice, it is possible, in principle, to synthesize jets over a broad range of length scales [e.g., synthetic jets having a nominal orifice dimension of 150 μm were fabricated using standard silicon micromachining techniques by Coe et al. (1994, 1995), and more recently Muller et al. (2001) reported microfabricated jet arrays].

The oscillating (time-reversed) pressure drop across an orifice that is necessary to form a synthetic jet can be imposed by an acoustic field, provided that the amplitude of the pressure oscillations is large enough to induce the time-periodic roll-up and subsequent advection of discrete vortices. The impulse that is imparted to each vortex has to be large enough to overcome the influence of both the orifice image and the forces associated with the (reversed) suction flow. Ingard & Labate (1950) used standing waves in an acoustically driven circular tube to induce an oscillating velocity field in the vicinity of an end plate and observed the formation of zero-net mass flux jets from opposing trains of vortex rings on both sides of the orifice. In a later experiment, Lebedeva (1980) created a round jet with velocities of up to 10 m/s, by transmitting high-amplitude sound waves through an orifice placed at the end of a tube. In a related investigation, Mednikov & Novitskii (1975) reported the formation of a jet without net mass flux and average streaming velocities of up to 17 m/s, by inducing a low-frequency (10–100 Hz) oscillatory velocity field at the end of a conical resonating tube driven by a piston and bellows mechanism.

Streaming motions without mass addition can also be effected by the transmission of sound through the flow field (often referred to as acoustic streaming) or by oscillating the boundary of a quiescent medium. Although these streaming flows are produced without net mass flux, they are not typically accompanied by the formation of discrete vortices that are inherent in the formation of synthetic jets by fluid injection through an orifice. As noted by Lighthill (1978), the streaming motions induced by acoustic waves result from the dissipation of acoustic energy or

the attenuation of the transmitted sound. Such attenuation can occur either within the body of the fluid (i.e., away from solid surfaces) at very high frequencies or owing to viscous effects near a solid boundary. Streaming motions associated with moving (oscillating) solid boundaries have been the subject of a number of investigations, most notably the time-harmonic oscillations of a cylinder normal to its axis (e.g., Stuart 1966, Davidson & Riley 1972, Riley & Wibrow 1995). Davidson & Riley demonstrated streaming velocities on the order of 1 cm/s in water at a nominal oscillation frequency of 45 Hz.

James et al. (1996) investigated the evolution of a synthetic round turbulent jet that is formed in water without an orifice by a submerged oscillating diaphragm that is flush mounted in a flat plate. These jets are produced without mass injection normal to and at the center of the diaphragm and are comprised entirely from radially entrained fluid. The jets are formed only when small clusters of cavitation bubbles appear and subsequently collapse near the center of the diaphragm during each oscillation cycle. The authors conjectured that the time-periodic formation of these bubbles displaces vorticity from the actuator's boundary layer and leads to the formation of nominally axisymmetric turbulent vortices (e.g., Kovasznay et al. 1973) that coalesce to synthesize a turbulent jet. Similar to a conventional turbulent round jet, the time-averaged width and the inverse of the centerline velocity of this synthetic jet increase linearly with the distance from the actuator.

In recent years, plane and round synthetic jets that are formed by time-periodic alternate ejection and suction of the working fluid through an orifice in the flow boundary have been investigated both experimentally (Smith & Glezer 1997, 1998; Smith et al. 1999; Mallinson et al. 1999; Crook et al. 1999, 2001; Rediniotis et al. 1999; Chen et al. 2000; Muller et al. 2000, 2001) and numerically (Kral et al. 1997; Rizzetta et al. 1998; Guo & Kral 2000). These investigations have emphasized a compact flow generator in which the orifice forms one of the surfaces of an otherwise sealed shallow cavity where the flow is driven by the motion of a diaphragm (or a piston) that is built into one of the cavity walls. For a given actuation input, the effectiveness of the flow generator can be maximized when the diaphragm and cavity are driven at a coupled resonance that depends on both the cavity flow (and geometry) and the structural characteristics of the diaphragm.

The investigations of Smith & Glezer (1997, 1998) have shown that, near the jet exit plane, the synthetic jet flow is dominated by the time-periodic formation, advection, and interactions of discrete vortical structures (e.g., vortex pairs or vortex rings), which ultimately become turbulent, slow down, and lose their coherence. Owing to the suction flow, the time-averaged static pressure near the exit plane of a synthetic jet is typically lower than the ambient pressure and both the streamwise and cross-stream velocity components reverse their direction during the actuation cycle. The time-periodic reversal in flow direction along the jet centerline (between the blowing and suction strokes) leads to the formation of a stagnation point on the centerline downstream of the orifice and confines the suction flow to a narrow domain near the exit plane. These features as well as the celerity and characteristic

length scale of the discrete vortices that form the jet can be varied over a broad range by the amplitude and period of the diaphragm motion.

The interaction of a synthetic jet (or jet arrays) with an external cross flow over the surface in which they are mounted can displace the local streamlines and induce an apparent or virtual change in the shape of the surface and is, therefore, of considerable interest for flow control applications. The control of aerodynamic flows by modifying the apparent shape of aerosurfaces in order to prescribe the streamwise pressure distribution and thereby influence their aerodynamic performance is not new and was addressed in several investigations in the 1940s and 1950s. For example, Perkins & Hazen (1953) used a stationary trapped vortex to alter the apparent local surface curvature and therefore the direction of the external flow near the trailing edge of an airfoil to increase the lift at zero angle of attack. In a recent investigation of the evolution of synthetic jets on the surface of a two-dimensional cylinder, Honohan et al. (2000) demonstrated that when the jets are operated on a timescale that is well below the characteristic timescale of the base flow, the formation of a quasi-steady interaction domain near the surface is accompanied by a more favorable pressure gradient. As a result, the surface boundary layer downstream of this domain becomes thinner allowing the flow to overcome stronger adverse pressure gradients and therefore delaying (or altogether suppressing) flow separation.

The unique attributes of synthetic jets coupled with the development of actuators that can be integrated into the flow surface without the need for complex piping and fluidic packaging make them attractive fluidic actuators for control of both external and internal flows. As noted above, apparent surface modification is typically implemented by operating the jet actuator on timescales that are below the characteristic timescale of the base flow. However, the unsteady effects of the actuation can also be coupled to inherent instabilities of the base flow to affect significant global modifications on scales that are one to two orders of magnitude larger than the characteristic length scales of the jets themselves. The utility of synthetic jets for flow control was demonstrated in the vectoring of conventional jets in the absence of extended control surfaces by Smith & Glezer (1994, 1997) and, in more detail, by Smith (1999). Since then, this approach to flow control has been adopted in a number of other applications, including the modification of the aerodynamic characteristics of bluff bodies (Amitay et al. 1997, 1998), control of lift and drag on airfoils (Kral et al. 1997; Smith et al. 1998; Amitay et al. 1999, 2001; Seifert & Pack 1999), reduction of skin friction of a flat-plate boundary layer (Lorkowski et al. 1997), mixing in circular jets (Davis & Glezer 1999), and control of internal flow separation (Amitay et al. 2000) and of cavity oscillations (Fabris & Williams 1999, Lamp & Chokani 1999).

The present review paper comprises two primary parts. In Section 2, the formation and the near- and far-field evolution of isolated synthetic jets (i.e., in the absence of a cross flow) are discussed. Section 3 focuses on the evolution of the interaction domain between a synthetic jet and a cross flow on the surface of a two-dimensional cylinder and the modification of the base flow.

2. ISOLATED SYNTHETIC JETS

2.1. Jet Formation

An isolated synthetic jet in the absence of a cross flow is produced by the interactions of a train of vortices that are typically formed by alternating momentary ejection and suction of fluid across an orifice such that the net mass flux is zero. Whereas the nominally axisymmetric (or two-dimensional) flow during the suction stroke may be thought of as similar to the flow induced by a sink that is coincident with the jet orifice, the flow during the ejection stroke is primarily confined to a finite narrow domain in the vicinity of the jet centerline. During the momentary ejection, the flow separates at the sharp edges of the orifice and forms a vortex sheet that typically rolls into a vortex (vortex rings or vortex pairs for circular or two-dimensional orifices, respectively) that moves away from the orifice under its own self-induced velocity (e.g., Auerbach 1987). The degree of interaction between the vortex and the reversed flow that is induced near the orifice by suction of makeup fluid when the pressure drop across the orifice is reversed depends on the strength (i.e., impulse) of the vortex and its distance from the orifice.

As noted in Section 1, synthetic jets are typically formed by imposing a time-periodic alternating pressure drop across an orifice (e.g., by acoustic waves or by the motion of a piston or a diaphragm). Recent investigations have employed a variety of jet drivers including piezolectrically driven diaphragms (e.g., Smith & Glezer 1997, 1998; Mallinson et al. 1999; Crook et al. 1999; Chen et al. 2000), electromagnetically driven pistons (e.g., Rediniotis et al. 1999, Crook & Wood 2001), and acoustically driven cavities (e.g., Erk 1997, McCormick 2000, Kang et al. 2000). Crook et al. (1999) modeled the coupled structural and fluid characteristics of a synthetic jet generator that employed a piezoelectrically driven diaphragm. The flow was modeled using the unsteady Bernoulli equation, and the effects of the orifice diameter and the cavity height on the jet flow were evaluated. Although the agreement between the predicted and measured dependence of the centerline velocity on orifice diameter and cavity height is poor, the trends are similar. More recently, Chen et al. (2000) characterized piezoelectrically driven synthetic jet actuators using a variety of piezoceramic disc elements having different mechanical properties and varying thickness and diameter.

The complex flow field within the actuator cavity has been primarily treated numerically. For example, Rizzetta et al. (1998) used the unsteady compressible Navier-Stokes equations for numerical simulations of both the flow within the actuator cavity and the jet flow near the orifice where the time harmonic motion is driven by a moving wall (opposite to the orifice). Two-dimensional simulations were conducted for either a fixed Reynolds number or a fixed cavity height. During the suction stroke, a counter-rotating vortex pair is formed at the inner edges of the orifice, impinges on the opposite wall, and dissipates near the center of the cavity (ostensibly owing to the injection of opposite sense vorticity from the wall boundary layer) before the next ejection cycle begins. For a given Reynolds number, the strength of the vortex pairs that are produced on both sides of the orifice

appears to increase with decreased cavity height (as was also confirmed in a later investigation by Lee & Goldstein 2000). A comparison between time-averaged velocity distributions downstream of the orifice of both two-dimensional and separate three-dimensional simulations and the earlier measurements of Smith & Glezer (1997) yielded a reasonable agreement near the jet centerline.

In the work of Smith & Glezer (1998), a nominally high aspect ratio ($AR = 150$) two-dimensional synthetic jet is formed in air through a rectangular orifice (0.5 mm wide) in a shallow (and otherwise sealed) cavity by piezoelectric diaphragms that are mounted on one of the cavity walls (Figure 1*a*) and are driven at resonance (nominally 1140 Hz). A Schlieren image in the *x-y* plane of the jet that extends approximately through $x/b = 70$ (Figure 1*b*) shows a vortex pair that is formed near the orifice as well as the outline of a turbulent jet farther downstream. Although the vortex pair and the remainder of the ejected fluid appear to be laminar after the roll-up is completed, the cores of the vortex pairs become unstable and begin to break down to small-scale motions around $t/T = 0.5$ (i.e., at the beginning of the suction flow). Similar to an isolated vortex ring (Glezer 1988), the onset of small-scale transition appears to take place near the front stagnation point of the vortex pair where the strain rates are high. Based on the Schlieren visualization, the transition process seems to proceed toward the rear of the vortex and ultimately progresses through the fluid stem behind it.

Axisymmetric vortex rings (e.g., Didden 1979, Glezer 1988) may be characterized by two primary dimensionless parameters. The first parameter is the dimensionless "stroke" length $L_0/d (L_0 = \int_0^\tau u_0(t)dt$, where $u_0(t)$ is the streamwise velocity (averaged over the area of the orifice), τ is the time of discharge, and d is the characteristic length scale of the orifice. The second parameter is the Reynolds number based on the impulse (i.e., the momentum associated with the discharge) and is given by $Re_{I_0} = I_0/\mu d$, where $I_0 = \rho \int_0^\tau \int_A u_0^2(\overline{x}, t)dA\,dt$, where ρ and μ are the fluid density and viscosity, respectively. Alternative Reynolds numbers may be defined based on the circulation of the ejected fluid or the time-averaged orifice velocity during the ejection. For noncircular orifices, the aspect ratio of the orifice may influence the out-of-plane distortion of the vortices and hence their streamwise advection and evolution (e.g., Dhanak & Bernardinis 1981) and ultimately the streamwise variation of the jet cross section (e.g., Ho & Gutmark 1987). When the vortices are generated time-periodically to synthesize a jet, an important formation parameter is the repetition rate or the formation frequency f, where the dimensionless frequency $F^* = f I_0/(\rho \nu^2)$ is a measure of the total impulse per unit time and thus may be used as a parameter that characterizes different jets according to their strength. Other formation parameters may include the formation duty cycle (i.e., τ/T) and an integral formation parameter that accounts for different velocity programs during the ejection and suction strokes. The characterization of the formation parameters of the jet is simplified when the jet is driven time-harmonically, and the formation parameters depend primarily on the frequency and amplitude of the driving mechanism (e.g., diaphragm or piston motion) and cannot be varied independently.

Some details of the formation of the jet vortices were studied by Rediniotis et al. (1999) in a circular jet ($D = 2$ mm) driven by a shaker. For a given Reynolds number ($Re_D = 200$), the authors observed the formation of a jet for $L_0/D = 1.6$ and $St = 0.2$ (based on the maximum exit velocity); while for $L_0/D = 0.16$ and $St = 2$, the ejected fluid was drawn back into the cavity during the suction stroke and therefore no jet was formed. [In experiments on the formation of vortex rings in the absence of suction, Didden (1979) noted that isolated vortex rings could not be produced for $L_0/D < 0.4$ over the same range of Reynolds numbers.] In related flow-visualization experiments, Crook & Wood (2001) investigated the formation and interaction of vortices within a round synthetic jet operating at 50 Hz (Figure 2). For four Reynolds numbers (between 660 and 2300, based on the peak velocity at the orifice) and corresponding L_0/D between 2.56 and 8.9, the vortices increase in size, and there is virtually no interaction between successive vortices. In fact, the turbulent vortices at $Re_D = 2300$ resemble isolated turbulent vortices, including the formation of secondary vortices within the wake, that were observed by earlier investigators (e.g., Glezer 1988). However, for a low Reynolds number ($Re_D = 330$, $L_0/D = 1.28$), the celerity of the successive vortices appears to be low enough so that the motion is apparently affected by the buoyancy of the tracer smoke particles.

2.2. Near-Field Evolution

It is clear that at least in the near field of the jet, its evolution depends critically on the details of the formation and advection of the discrete vortices in the presence of the time-periodic reversed flow. Smith & Glezer (1998) determined the celerity $U_c(x, t)$ of the vortex pairs (Figure 3*a*) from the time derivative of the phase-averaged trajectories of the cores of a family of nominally two-dimensional vortex pairs (for $1400 < I_0/\mu h < 30{,}000$ and a fixed actuator frequency). The trajectories of the vortex pairs appear to scale with L_0, and they are made up of three distinct domains that are characterized by substantial changes in the celerity. For $0.25 < t/T < 0.5$, the vortex pairs are nominally laminar and the celerity decreases like $(t/T)^{-0.5}$ (a straight line segment $m = -0.5$ is shown for reference). Based on flow visualization, Smith & Glezer (1998) noted that the vortex pair begins to undergo transition to turbulence approximately at the beginning of the suction cycle of the actuator, which may in fact be triggered by core instabilities associated with the reversal of the streamwise velocity near the exit plane. Following transition ($0.5 < t/T < 0.8$), $U_c(x, t)$ decreases like $(t/T)^{-2}$, which is faster than for the laminar vortex pair and considerably faster than for an isolated turbulent vortex. The celerity has a local minimum at $t/T \approx 0.8$ and then increases like $(t/T)^2$ until the vortex pair becomes indistinguishable from the jet flow and its fluid effectively moves with the mean flow of the jet. The authors noted that regardless of the total impulse, no vortices are phase locked to the actuator signal much beyond $t/T > 1.3$.

In addition to the time-averaged centerline velocity $U_{cl}(x)$ and the celerity, the evolution of the jet near the exit plane may also be characterized by the magnitude

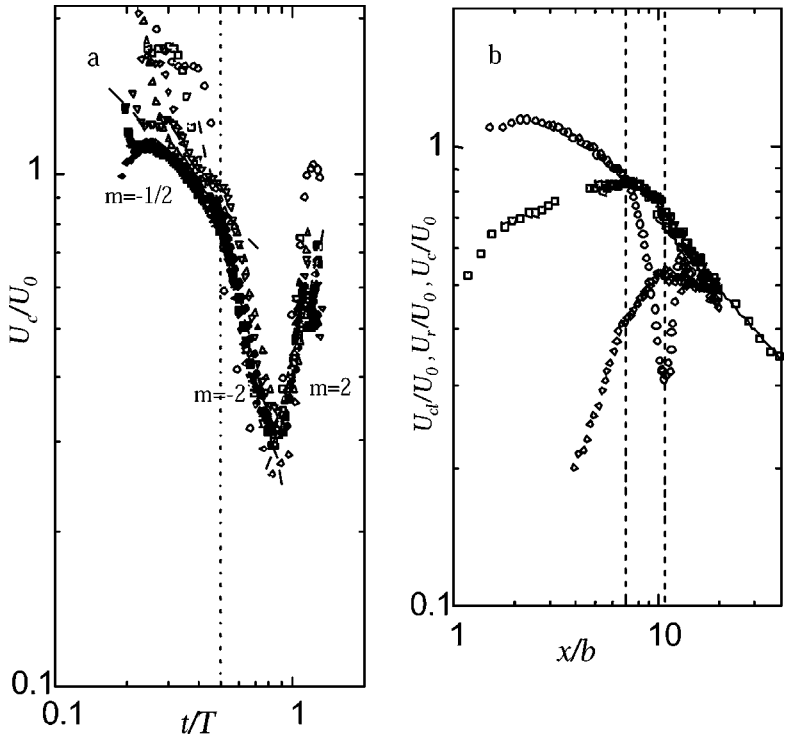

Figure 3 (*a*) Variation of vortex-pair celerity with time. $Re_{l_0} = 1{,}396$ (○), 3,171 (□), 4,967 (◊), 9,072 (△), 12,552 (▽), 18,124 (●), 20,761 (■), 22,282 (♦), 27,025 (▲), and 29,654 (▼); (*b*) Mean centerline velocity (□), celerity (○), and residual velocity (◊) for $Re_{l_0} = 18{,}124$ ($Re_{U_0} = 383$). From Smith & Glezer (1998).

of the phase-averaged (relative to the actuation signal) residual centerline velocity between (i.e., before or after the passage of) successive vortices at a given streamwise location. This residual velocity $U_r(x)$ is, in part, a measure of the time-invariant velocity of fluid that is entrained into the jet column by the suction flow that is induced at the orifice. Figure 3*b* shows the streamwise variation of $U_c(x)$, $U_r(x)$, and $U_{cl}(x)$ in the near field (for $\mathrm{Re}_{l_0} = 18{,}124$) and shows that both the celerity and the centerline velocity decrease substantially during transition to turbulence (around $x/b = 7$). Furthermore, the celerity and the residual velocity become equal to the time-averaged centerline velocity for $x/b > 20$. However, the centerline velocity decreases like $x^{-0.58}$ (compared to $x^{-0.5}$ for conventional two-dimensional turbulent jets) ostensibly as a result of the variation of the static pressure in the vicinity of the orifice and the finite aspect ratio of the jet.

The time-periodic reversal in flow direction along the jet centerline during the blowing and suction strokes leads to the time-periodic appearance of a stagnation (saddle) point on the centerline (between the recent vortex and the jet exit plane) that

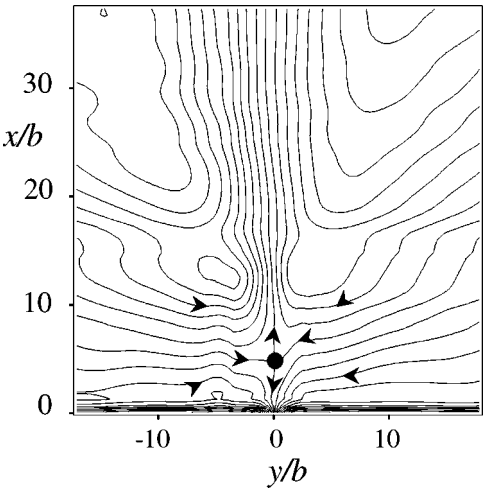

Figure 4 Phase-averaged streamline maps computed (at $t/T = 0.75$) from particle image velocimetry (PIV) data. $f = 600$ Hz, $Re_{U_0} = 300$, and $L_0/b = 29.1$.

moves along the centerline during the suction stroke. The presence of a stagnation point in phase-averaged streamline maps of a two-dimensional jet (Figure 4) that are computed from particle image velocimetry (PIV) data is shown by B.L. Smith and A. Glezer (submitted). The stagnation point is located at $x/b = 5$ and the stagnation streamlines on both sides of the stagnation point separate between the flow that is driven by the ejection stroke and the suction flow (toward the jet orifice). The latter is restricted to the domain that is also bounded by the exit plane of the jet and is nominally symmetric with respect to the jet centerline. The streamline map also shows that the flow downstream of the branches of the stagnation point on both sides of the centerline is directed toward the jet orifice and then turns around in the streamwise direction near the cross-stream edges of the jet. These authors also noted that the symmetry of the flow that is transported toward the orifice during the suction stroke can be altered on either side of the jet centerline by extending one of the edges of the jet orifice in the downstream direction (the length of the extension is of the order of the orifice width) thus restricting the suction flow on that side and increasing the flow rate on the opposite side of the jet orifice. As shown by the authors, the ability to control the symmetry of the suction flow plays an important role in the vectoring of conventional jets by synthetic jet actuators.

2.3. Far-Field Evolution

The works of Smith & Glezer (1997) and Smith et al. (1999) in a two-dimensional jet show that although cross-stream distributions of the time-averaged streamwise and cross-stream velocity components and the corresponding rms velocity

fluctuations appear to collapse in the usual similarity coordinates, the streamwise scaling of other variables (e.g., the centerline velocity, jet width, volume flow rate, etc.) do not match corresponding scaling for conventional jets. For example, whereas the width b of a two-dimensional synthetic jet varies like $x^{0.88}$ ($b \propto x$ for a conventional two-dimensional jet), $\mathrm{d}b/\mathrm{d}x$ is almost twice as large as in conventional jets at much higher Reynolds numbers (of order 10^4, e.g., Heskestad 1965). Furthermore, even though the streamwise variation of the jet volume flow rate $\mathrm{d}Q/\mathrm{d}x$ is smaller than in conventional jets, the net entrained volume flow rate of the synthetic jet within the domain $x/b < 80$ is nearly $4Q_0$ ($Q_0 = U_0 b$) and substantially larger than for conventional jets (e.g., Kotsovinos & Angelidis 1991). The departure from conventional self-similarity is apparently associated with a streamwise decrease in the jet's momentum flux, which is typically assumed to be an invariant of the flow for conventional self-similar two-dimensional jets. This decrease in the momentum flux of synthetic jets is a result of the adverse streamwise pressure gradient near the jet orifice that is imposed by the suction cycle of the actuator and is manifested by a time-averaged static pressure, which is lower than the ambient.

In a related numerical investigation (using RANS) of an isolated two-dimensional synthetic jet, Kral et al. (1997) considered a two-dimensional incompressible synthetic jet flow where the unsteady flow from the harmonic motion of the actuator was modeled with blowing/suction boundary condition (the simulation did not take into account the details of the cavity flow). The numerical results for the streamwise variation of the centerline velocity as well as cross-stream distributions of the streamwise velocity were in good agreement with the earlier measurements of Smith & Glezer (1997).

It appears that the far-field behavior of round synthetic jets is somewhat closer to that of conventional (turbulent) round jets. For example, Mallinson et al. (1999, 2000) reported a good agreement between measured and computed streamwise variation of the centerline and cross-stream velocity distributions and that the centerline velocity decays like $1/x$ (as in conventional round jets) (Figure 5). Muller et al. (2000, 2001) focused on the thrust produced by a synthetic round jet over the range $200 < Re_{I_0} < 2000$. They showed that the jet performance depends on L_0/D and identified two flow regimes. For $L_0/D < 3$, the thrust increases like L_0^4 and is smaller than the momentum flux of the ejected fluid, ostensibly as a result of the reingestion of some of the vorticity during the suction stroke. However, for $L_0/D > 3$, the thrust is proportional to L_0^2 and is equal to the momentum flux of the ejected fluid. These authors also showed that, unlike two-dimensional jets, the entrainment rate of the round synthetic jet is comparable to a conventional axisymmetric turbulent jet.

Velocity spectra of synthetic jets are characterized by the rapid streamwise attenuation of spectral components above the formation frequency of the jet thus indicating strong mixing and dissipation within the jet and reduction in the total turbulent kinetic energy (Smith & Glezer 1998). Power spectra of the centerline velocity of the two-dimensional jet in Figure 3 are shown in Figure 6*a–c* (measured at $x/b = 5.9$, 19.7, and 177.2, respectively). Near the jet exit plane (Figure 6*a*),

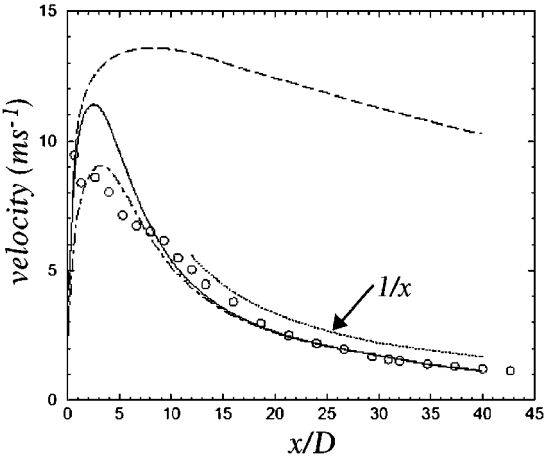

Figure 5 The streamwise variation of the jet centerline velocity (from Mallinson et al. 1999). Experiments (○), laminar computation (--), turbulent computation (—), corrected turbulent computation (–●–).

the spectrum is dominated by the formation frequency and its higher harmonics (hot-wire rectification within this domain also adds higher harmonics), whereas the spectral distribution below the fundamental frequency is virtually featureless. The harmonics of the formation frequency are rapidly attenuated with downstream distance and by $x/b = 19.7$; only the fundamental and its first harmonics are present, and there is a significant increase in the magnitude of the spectral band below the formation frequency. Therefore, following the time-harmonic formation of the discrete vortex pairs, energy is transferred from these primary ("large-scale") eddies, which coalesce to form the jet, both to the mean flow and to smaller scales at which dissipation ultimately takes place. It is remarkable that the spectral band below the formation frequency (with the exception of a weak spectral band around 10 Hz) remains featureless and shows no evidence of subharmonics of the formation frequency (and thus of pairing interactions between the jet vortices). Subharmonic frequencies were present in the DNS of a two-dimensional synthetic jet of Lee & Goldstein (2000) who showed evidence of vortex pairing at low Reynolds numbers (based on the jet peak velocity). However, these authors noted that the pairing interactions might have been the consequence of the closed streamwise-periodic simulation domain.

A striking feature of the velocity spectra in Figures 6*b*,*c* is the rapid streamwise attenuation of high spectral components indicating strong dissipation within the synthetic jet and a reduction in the total turbulent kinetic energy. By $x/b = 177$ (Figure 6*c*), the nominal magnitude of the band $f < 100$ Hz is comparable to the corresponding band near the jet exit plane (suggesting energy transfer to the smaller scales) and at the same time, the "rollover" frequency moves toward lower frequencies. The spectral distributions in Figures 6*b*,*c* also include a relatively narrow

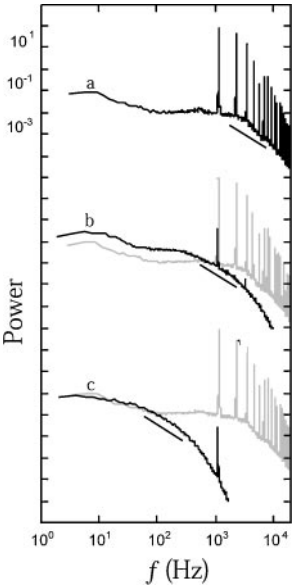

Figure 6 Power spectra of the centerline velocity (Smith & Glezer 1998). Each curve is successively displaced 7 decades: (*a*) $x/b = 5.9$, (*b*) 19.7, and (*c*) 177.2; $Re_{U_0} = 383$.

frequency band having a slope of approximately $-5/3$, suggesting the existence of an inertial subrange, which is limited by the (global) low Reynolds number of the flow. It is noteworthy that because the characteristic local (centerline) velocity decreases with downstream distance the spectral peak at the formation frequency actually shifts toward higher wave numbers where the dissipation ultimately takes place.

3. INTERACTION OF SYNTHETIC JETS WITH A CROSS FLOW

3.1. Global Effects

Some fundamental features of virtual aerodynamic modification of bluff bodies are investigated in the flow around a circular cylinder in a uniform cross stream. This base flow provides a unique opportunity to place the jet at various azimuthal positions having different local pressure gradients and to investigate its global effect on the flow field and the aerodynamic forces on the model. The interaction between the jets and the cross flow over the cylinder model were first investigated in a flow visualization study (Amitay et al. 1997) in a small, two-dimensional smoke tunnel ($Re_D = 4000$) for a number of azimuthal jet positions (Figure 7*a–d*). The

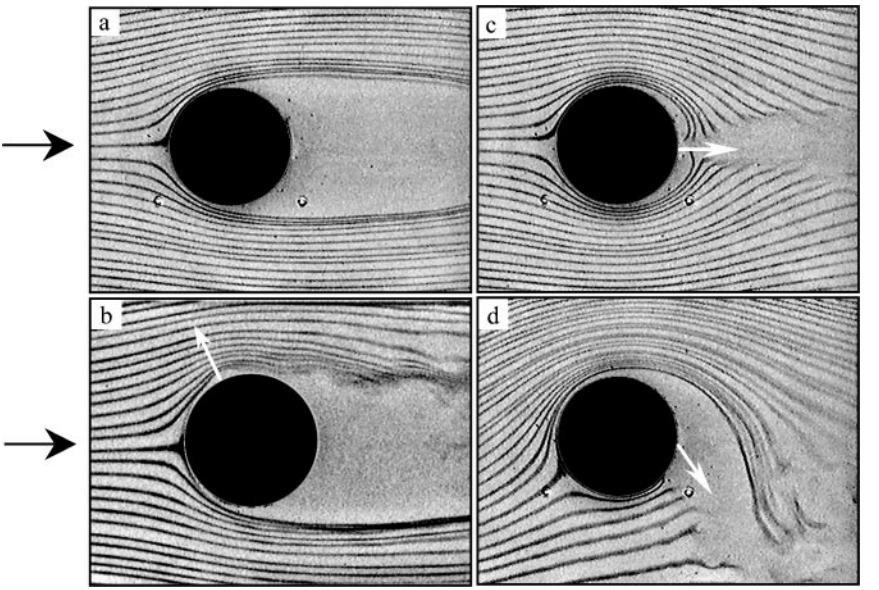

Figure 7 Smoke of the flow around a circular cylinder visualization: (*a*) baseline; and (*b*) actuated: $\phi = 0$, $\gamma = 60^\circ$ and (*c*) 180°, and (*d*) $\phi = 120^\circ$, $\gamma = 180^\circ$.

center section of a cylinder model ($D = 62$ mm) is instrumented with a pair of adjacent rectangular synthetic jet actuators (0.5 × 140 mm) that are spaced 2.5 mm apart along the long side of their orifices and are flush with the cylinder surface and collinear with its axis. The azimuthal jet location relative to the front stagnation point γ is varied by rotating the cylinder around its axis and the actuation level is characterized using the momentum coefficient $C_\mu = \overline{I}_j / \frac{1}{2}\rho_0 U_0^2 D$, where $\overline{I}_j$ is the time-averaged jet momentum per unit length during the outstroke and ρ_0 is the free-stream fluid density.

The baseline flow (the flow is from left to right) is shown for reference in Figure 7*a* and appears to separate at $\theta \sim 80^\circ$ (for reference below, the streamwise line of symmetry is denoted the x axis). When the jets are placed at $\gamma = 60^\circ$ (Figure 7*b*) and are operated in phase so that the combined C_μ is O(10^{-3}), the effect on the cross flow is manifested by a (relatively small) local deformation of smoke streaklines above the top surface of the cylinder. Although the changes in the external flow are somewhat subtle, it is apparent that the separation point on the top surface moves downstream and that the front stagnation point is displaced below the x axis (i.e., toward the bottom of the cylinder). Other visualization images show that the cross-stream symmetry of the cylinder wake can be substantially altered when the jets are placed in the azimuthal domain $100^\circ < \gamma < 180^\circ$ for increased levels of C_μ (Amitay et al. 1997) and can induce the formation of two uneven closed recirculating regions. When the jets are placed at $\gamma = 180^\circ$ and

C_μ is increased to O(10^{-1}) (Figure 7*c*), the external flow appears to be almost attached to the surface of the cylinder. Finally, in Figure 7*d*, the jets are still placed at $\gamma = 180^\circ$, but they are operated out of phase such that the bottom jet is leading by $2\pi/3$. [As shown by Smith & Glezer (1998), Smith et al. (1999), and more recently investigated numerically by Guo & Kral (2000), out-of-phase operation of adjacent synthetic jets results in vectoring of the combined jet toward the jet that is leading in phase.] The vectoring of the jets results in downward deflection of the entire wake and a concomitant displacement of the front stagnation point, which is qualitatively similar to classical flow visualization snapshots of the flow around a spinning cylinder. The decrease and increase in the spacing between streaklines above and below the cylinder, respectively, are indicative of a change in circulation and generation of lift.

In larger-scale experiments, Williams et al. (1991) used time-harmonic bleed out of a narrow spanwise slot in a cylindrical shell driven by an internal high-power speaker [$21{,}000 < Re_D < 55{,}000$ and $0.1 < St < 1.5$, and a bleed coefficient $C_b = \mathrm{O}(0.1)$] to investigate the effect of the forcing frequency of unsteady bleed on the pressure distribution around the cylinder where the azimuthal location of the slot was varied upstream and downstream of separation. The most salient feature of the actuated flow was a local variation in the azimuthal pressure distribution (primarily downstream of the jet) that suggests an increase in lift (but in some cases also an increase in form drag). Their data also suggest that when actuation was applied near the location of separation (in the absence of actuation), the separation point moved as far downstream as $\theta \approx 120^\circ$. Williams et al. (1991) also reported that the local minimum in the pressure coefficient downstream of the excitation slot scaled with C_b (which is proportional to the conventional momentum coefficient C_μ), and that for a given bleed coefficient the effect of the excitation is essentially independent of the forcing frequency.

Detailed azimuthal pressure distributions on the surface of the cylinder described in connection with Figure 7 were measured by Amitay et al. (1997) in a series of wind tunnel experiments at considerably higher Reynolds numbers (up to 131,000) but substantially lower levels of momentum coefficient [$C_\mu \sim \mathrm{O}(10^{-4})$]. The actuation frequency is deliberately selected to be well above the natural shedding frequency of the cylinder (typically $St \approx 0.2$), and at $Re_\mathrm{D} = 75{,}500$ ($C_\mu = 6 \cdot 10^{-4}$) the actuation Srouhal number is approximately 2.5. The azimuthal distributions of the pressure coefficient $C_p(\theta)$ on the surface of the cylinder for the baseline and actuated configurations at several actuator angles γ (each marked with a dashed line) are shown in Figure 8*a–c*. At this level of C_μ, the effect of the jets on the pressure distribution is noticeable for $\gamma > 15^\circ$. When $\gamma = 45^\circ$ (Figure 8*a*), there is already a global change in $C_p(\theta)$ around most of the circumference of the cylinder. The pressure coefficient decreases both upstream and downstream of the actuator relative to the baseline flow between the front stagnation point, and $\theta \approx 120^\circ$ (where the flow appears to separate) with a local minimum around $\theta \approx 75^\circ$ indicating a nonzero lift force. Of particular note is the almost uniform increase in the base pressure of the cylinder between the top and bottom separation points indicating a decrease in pressure drag (see also Figure 9*b*). As γ is

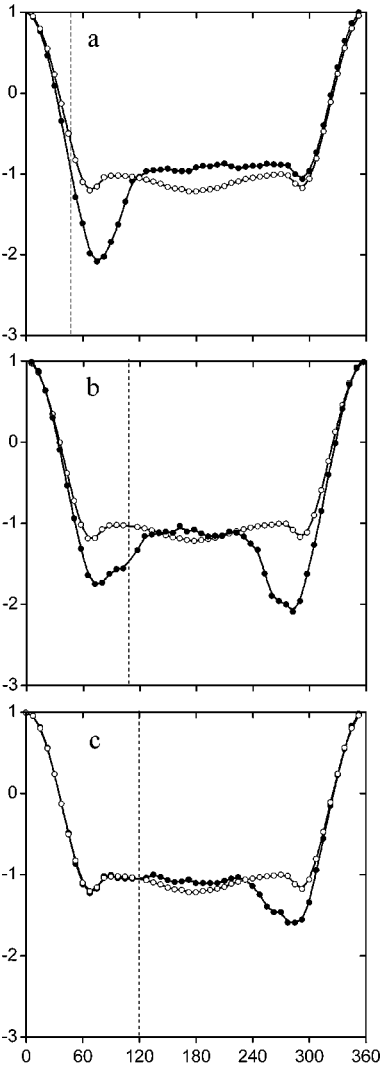

Figure 8 Azimuthal variations of C_p at $Re_D = 75{,}500$ (○) baseline and (●) actuated. The dashed lines mark the jet location: (*a*) $\gamma = 45°$, (*b*) 110°, and (*c*) 120°.

increased, the pressure on the top surface continues to decrease (when $\gamma = 100°$, the pressure minimum almost reaches the potential flow value $C_p = -3$) and the separation point moves farther downstream (up to 125°). It is noted that similar asymmetric pressure distributions were measured in the absence of actuation at $Re_D = 360{,}000$ (Shih et al. 1993) where the asymmetry resulted from one-sided turbulent reattachment. At this Reynolds number, the flow apparently tends to be bi-stable and may even exhibit hysteresis (Schewe 1983).

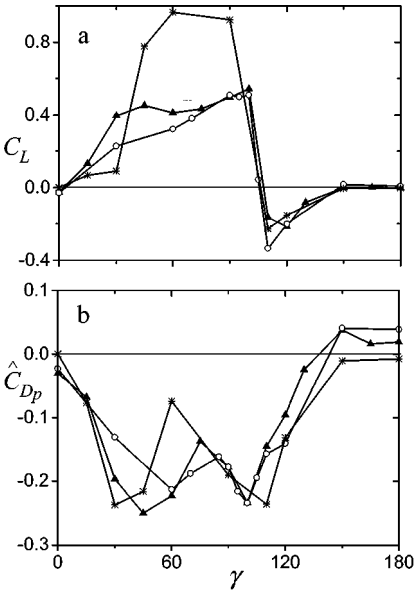

Figure 9 Variations of (*a*) C_L and (*b*) C_{D_p} with jet angle. (○) $Re_D = 75{,}500$, $St = 2.6$, (▲) $Re_D = 75{,}500$, $St = 4.5$, (*) $Re_D = 131{,}000$, $St = 1.49$.

Perhaps the most prominent feature in the pressure distributions when $\gamma > 100^\circ$ (Figures 8*b,c*) is the appearance of a local minimum in the static pressure on the unactuated (lower) half of the cylinder upstream of the separation point, which offsets the increase in lift. When $\gamma = 110^\circ$ (Figure 8*b*) the two pressure minima and the rest of the pressure distributions on the top and bottom surfaces are almost symmetric, indicating that at this actuator angle the lift is approximately zero. As γ is further increased to 120° (Figure 8*c*) the pressure distribution upstream of the actuator on the actuated side is almost indistinguishable from the pressure distribution of the baseline flow. However, the suction induced by the jets in the base region appear to delay separation on the opposite (bottom) half of the cylinder, indicating a reversal in the direction of the lift force.

The variations of the lift coefficient C_L and of the normalized increment in (pressure) drag $\hat{C}_{D_p}(\hat{C}_{D_p} = C_{D_{Pactuated}}/C_{D_{Pbaseline}} - 1)$ with azimuthal jet position are shown in Figure 9*a,b*, respectively for two Reynolds numbers and actuation frequencies. At least for these experimental conditions, the distributions of C_L and $\hat{C}_{D_p}$ appear to be only weakly dependent on the actuation frequency. At both frequencies, $\hat{C}_{D_p}$ decreases (i.e., a decrease in the pressure drag), whereas C_L increases with γ. At $Re_D = 75{,}000$, the maximum lift coefficient is approximately 0.54, and at $Re_D = 131{,}000$ the lift coefficient reaches a maximum of 0.93 [in the experiments of Shih et al. (1993), at $Re_D = 360{,}000$ the lift coefficient was 1.6]. As noted in connection with the pressure distribution in Figure 8*c*, the lift

force reverses its direction for $\gamma > 100^\circ$ and ultimately vanishes at $\gamma = 135^\circ$. These measurements also showed that, for the range $60^\circ \leq \gamma \leq 90^\circ$, C_L and $\hat{C}_{D_p}$ are relatively insensitive to variations in C_μ for $C_\mu > 10^{-4}$.

A localized delay of separation of a (tripped) turbulent boundary layer on the surface of a circular cylinder ($Re_D = 550{,}000$) downstream of a single round synthetic jet (d = 1.2 mm) placed just upstream of the separation line was investigated by Crook et al. (1999). The jet was driven with and without amplitude modulation (the modulation frequency was equal to the natural shedding frequency). Oil film flow visualization indicated entrainment of the surrounding fluid toward the jet actuator and a localized delay of separation. In a related investigation, Rediniotis et al. (1999) used a two-dimensional tangential synthetic jet for delaying separation over a circular cylinder in a water tunnel ($Re_D = 6{,}600$). By placing the jet immediately downstream of the separation line (in the absence of actuation) and operating it at near the natural unstable frequency of the separating shear layer, the authors were able to delay separation and asserted that this delay was caused by increased mixing within the cylinder boundary layer.

The modification of the aerodynamic forces on the cylinder is accompanied by substantial changes in the structure of its wake, as may be inferred from representative measurements of the cross-stream distributions of the time-averaged streamwise velocity and the Reynolds stresses (Amitay et al. 1998) shown in Figure 10. For the baseline configuration, the cross-stream distribution of the streamwise velocity is reasonably symmetric about the streamwise axis ($y/D = 0$), indicating that the lift coefficient is nearly zero. The effected lift and reduced pressure drag are accompanied by a cross-stream displacement of the wake as a result of an induced downwash (not shown) as well as a smaller velocity deficit within the wake (Figure 10*a*). The actuation also results in substantial reduction of the turbulent stresses across the entire wake (only $\overline{u'v'}$ is shown in Figure 10*b*), which may be attributed to the reduction in the scale of the shed vortices and enhanced dissipation that is caused by direct coupling of the excitation to the small-scale motions in the near wake (e.g., Wiltse & Glezer 1998). As shown by the power spectra of the streamwise velocity in Figure 11*a*, the actuation frequency of the jets is within the dissipation range of the near wake flow and substantially higher than the natural shedding frequency. Note that the distribution of $\overline{u'v'}$ in the actuated flow is not symmetric about the center of the wake and is somewhat higher on the (upper) actuated side (Figure 10*b*). Similar measurements of the effect of actuation when the cylinder's upper and lower boundary layers are deliberately tripped (symmetrically at $\theta = \pm 30^\circ$) show that the increase in lift and reduction in drag are also accompanied by a substantial reduction in the turbulent stresses within the wake.

Power spectra of the streamwise velocity measured on both sides of the wake at $x/D = 1$ and 3 where the streamwise velocity deficit is half the maximum deficit are shown in Figures 11*a,b*, respectively. The spectra of the baseline flow are dominated by a spectral peak at the (natural) shedding frequency (47 Hz), which increases in amplitude between $x/D = 1$ and 3. In the presence of actuation, the spectrum on the upper side of the wake includes a strong component at the

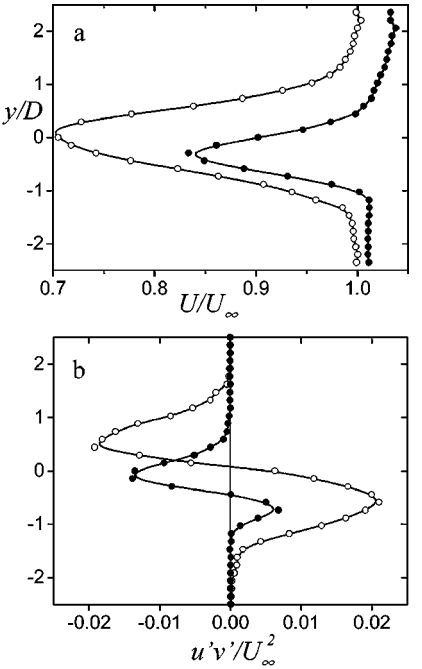

Figure 10 The cross stream distributions of the mean streamwise velocity (*a*) and the Reynolds stresses (*b*) at $x/D = 3$ for $Re_D = 75{,}500$, $C_\mu = 6 \cdot 10^{-4}$ and $\gamma = 60^\circ$. (○) baseline and (●) actuated.

actuation frequency (740 Hz), and the spectral peak at the shedding frequency and all other spectral component below the actuation frequency are strongly attenuated, suggesting enhanced transfer of energy from the large to small scales. On the bottom (unactuated) side of the wake, the shedding frequency increases to 80 Hz commensurate with the reduction in the cross-stream width of the wake. The magnitudes of the spectral peak at the shedding frequency and all other spectral components are smaller than in the baseline flow. At $x/D = 3$ (Figure 11*b*), the spectral component at the actuation frequency vanishes and the spectra on both sides of the wake are similar and include a spectral component at the higher shedding frequency (80 Hz). Furthermore, these data indicate that the turbulent kinetic energy throughout the entire spectrum of the actuated flow is lower on both sides of the wake, suggesting enhanced dissipation.

3.2. The Interaction Domain

For a given formation frequency and in the absence of a global length scale, the interaction domain between a synthetic jet and the cross flow near the jet orifice scales with the momentum flux ratio and the jet width (Honohan et al. 2000).

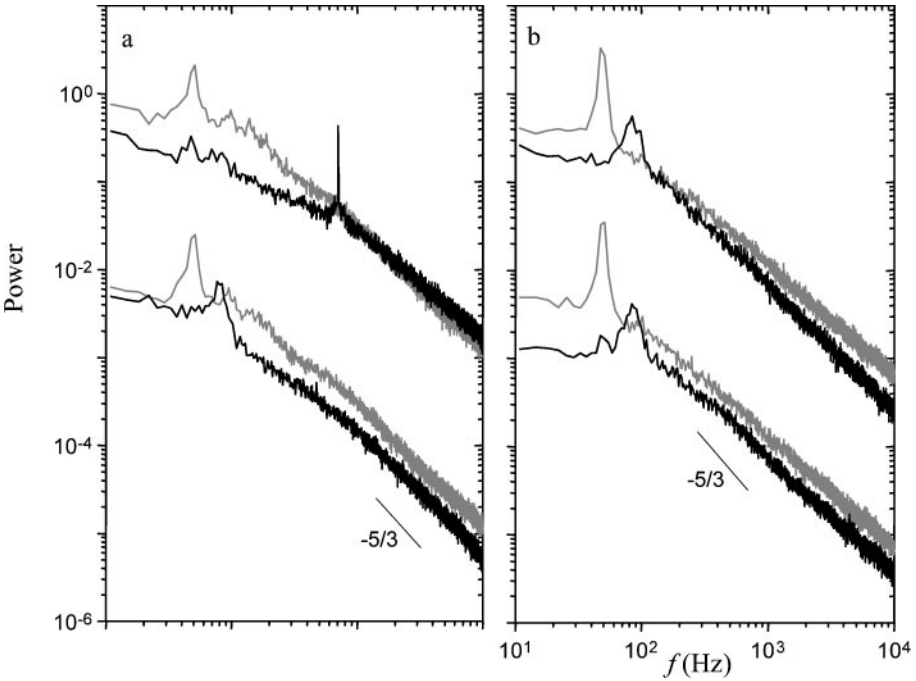

Figure 11 Power spectra measured at (*a*) $x/D = 1$ and (*b*) $x/D = 3$. The gray and black lines represent the baseline and actuated cases, respectively.

Depending on the formation frequency, the local free-stream velocity, and the dynamic pressure ratio between the jet and the cross flow, two distinct interaction domain are observed. These interaction regions alter the flow above the surface of the cylinder and thus its apparent aerodynamic shape. These regimes are mapped in terms of the dynamic pressure ratio (jet to cross flow) and the Strouhal number (based on jet width and free-stream velocity) and are shown in Figure 12. For a given dynamic pressure ratio, a closed recirculation region exists when the dimensionless frequency is larger than a critical value, and discrete vortices exist when this parameter is small. A dimensionless frequency $\hat{f}$ that is given by the product of the Strouhal number and the dynamic pressure ratio $(U_j/U_\infty)^2$ can be used as a delimiter between the two flow regimes, for example, the dashed line in Figure 12 corresponds to $\hat{f} = 0.1$.

Some details of the interaction between a two-dimensional jet mounted on a flat plate were investigated numerically by Palaniswamy (2001) in the vicinity of the jet orifice. The jet is 2 mm wide, with peak orifice velocity of 45 m/sec, and the speed of the uniform cross flow is 10 m/sec. The novel limited numerical scales (LNS) approach is a hybrid between RANS and LES in which small-scale flow features are resolved wherever computational grid is adequate and are diffused in

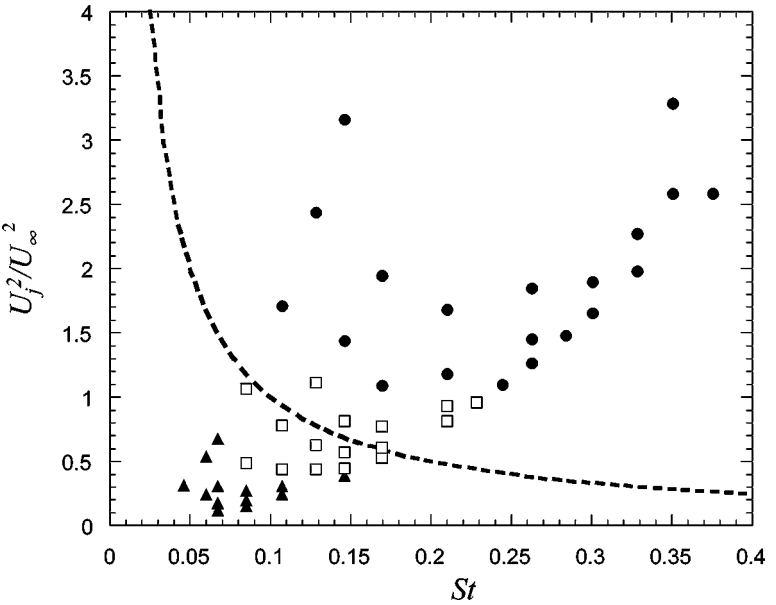

Figure 12 Interaction domain map. (▲) Discrete vortices, (□) transitory, (●) closed recirulation. Dashed line corresponds to $\hat{f} = 0.1$.

coarse parts of the mesh. Figure 13 presents a superposition of the velocity vector field and a color raster plot of the spanwise vorticity at four phase points of the actuation cycle. At the beginning of the ejection stroke ($t/T = 0$, Figure 13*a*), a (CW) vortex from the previous vortex pair is visible downstream of the orifice (note the vortex pair that forms inside the orifice during the suction stroke). At $t/T = 0.22$ (Figure 13*b*), the vortex pair associated with the current ejection stroke is tilted in the streamwise direction (the CCW vortex appears to be somewhat weaker ostensibly as a result of injestion of opposite-sense vorticity from the upstream boundary layer). During the next suction stroke of the cycle (Figure 13*c*), the vortex pair is removed from the orifice (their stems are drawn into the cavity), and the CCW vortex begins to roll over the CW vortex and toward the surface while it continues to weaken (and ultimately vanishes).

Distributions of the spanwise vorticity computed from several overlapping PIV data sets that are acquired along the surface of the cylinder (spatial resolution better than 0.15 mm) are shown in Figure 14 ($Re_D = 21{,}500$). The time-averaged vorticity in Figure14*a* shows that the baseline flow separates at $\theta \approx 85^\circ$. Phase-averaged vorticity maps in the presence of actuation (Figure 14*b*) show that the jet's vortex pairs interact with the wall boundary layer to form a train of clockwise (CW) vortical structures that are advected downstream, become weaker, and disappear within 3–4 wavelengths of the excitation ($\lambda = 0.5U_\infty/f$). These and other data (e.g., Figure 13) indicate that the (upstream) counterclockwise (CCW) jet

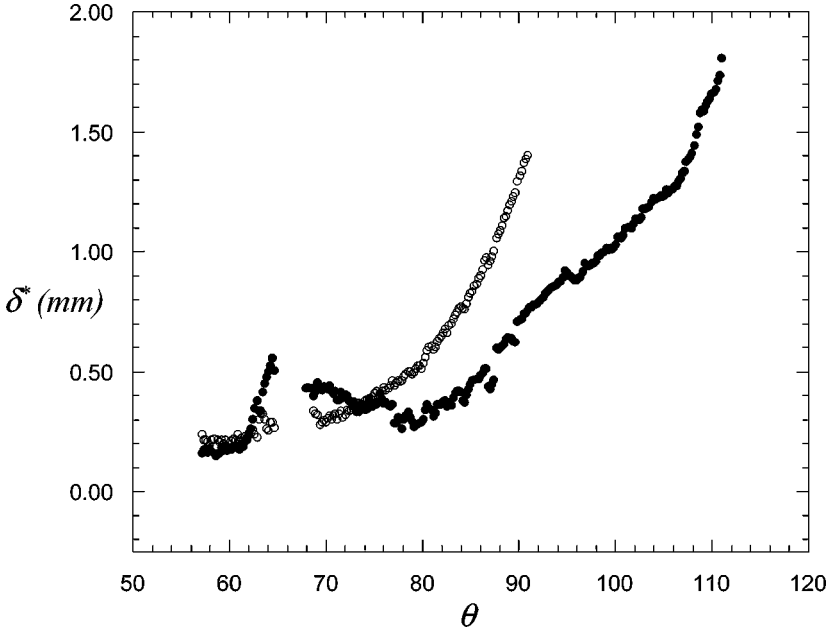

Figure 15 Boundary-layer displacement thickness $Re_D = 21{,}500$, $\gamma = 630$, $C_\mu = 5.1 \times 10^{-2}$, $\hat{f} = 0.035$. (○) baseline, (●) actuated.

vortex is accelerated above and around the CW vortex and rapidly weakens (within one wavelength). The image of the time-averaged actuated flow (Figure 14*c*) shows an interaction domain that protrudes into the cross flow above the edge of the local boundary layer in the absence of actuation (also see Figure 15) and ends approximately 2–3 λ downstream from the jet orifice followed by a thinner downstream boundary layer compared to the baseline flow. The evolution of the (time-averaged) boundary layer displacement thickness δ^* for the baseline and actuated flows are shown in Figure 15. Within the interaction domain, ($60^\circ < \theta < 80^\circ$), δ^* in the presence of actuation increases, reaches a local maximum immediately downstream of the jet, and then diminishes substantially, suggesting the presence of a favorable streamwise pressure gradient. For $\theta > 80^\circ$, δ^* begins to increase again, although at a lower streamwise rate than in the absence of actuation, until separation occurs at $\theta = 110^\circ$.

Local changes in the time-averaged pressure field that are caused by the interaction domain are computed from highly resolved PIV data sets. Figure 16 shows two streamlines having the same value of the stream function in the absence and presence of actuation superimposed with the vorticity distribution that is associated with the interaction domain between the jet and the cross flow (note the displacement of the streamline in the presence of actuation). The corresponding pressure distributions along the streamlines are shown in Figure 16*b*.

Compared to the baseline flow, in the presence of actuation, the pressure along the streamline is lower over the entire measurement domain, indicating an increase in the velocity along the streamline. More significantly, within the azimuthal sector that includes the interaction domain, there is a local minimum in the pressure distribution that indicates a significant favorable pressure gradient in the cross flow above the interaction domain. The favorable gradient is followed by a small region of weaker adverse pressure gradient, and finally, there is a slight favorable pressure gradient through the rest of the domain. As shown in Figure 15, the alteration of the streamwise pressure gradient results in a thinner boundary layer downstream of the interaction domain, and as a result, the separation occurs farther downstream. It is noted that Newman (1961) also reported a favorable pressure gradient downstream of the line of reattachment in a separating wall jet.

In addition to the downstream displacement of the separation domain, the interaction between the jet and the cross flow also has a profound effect on the separated shear layer. Figure 17 is a series of color raster plots of the time-averaged Reynolds stresses. The most striking feature in this figure is the diminution in magnitude of the Reynolds stresses within the separated shear layer as a result of the actuation. These data also accentuate the interaction domain where the largest contribution to the Reynolds stresses stems from the passage of the discrete vortices that are induced by the jet (e.g., Figure 14). The reduction of the Reynolds stresses within the separated shear layer of the actuated flow suggests that the delay in separation is not merely the result of a transition to turbulence in the surface boundary layer. Recent measurements have shown that the placement of a passive obstruction on the surface (instead of the jet) having a characteristic height $h/D = 0.014$ and a shedding frequency is similar to that of the jet and yields a similar interaction domain and similar levels of Reynolds stresses within the separating shear layer. Moreover, the cylinder lift and pressure drag associated with the passive obstruction are the same as in the presence of the jet.

3.3. Dynamic Response to Pulse-Modulated Actuation

The actuation discussed in the previous section is applied at frequencies that are typically higher than and decoupled from the "natural" unstable frequencies of the base flow (e.g., the shedding frequency), and therefore, its effect may be thought of as quasi-steady. In this section, we touch briefly on the transient effects of the actuation to assess the characteristic time of change in the global aerodynamic forces. Actuation is applied using pulse (top-hat) modulation of the actuator (resonant) waveform where the response time of the actuator itself is on the order of one actuation period.

As shown in Section 3.1, actuation at $\gamma = 45^\circ$ results in a positive lift force on the cylinder, which must be accompanied by a transient change in the vorticity flux with a net increase in circulation that is associated with the shedding of positive (CCW) vorticity. The measurements of Amitay et al. (1998) showed that, after the onset of modulation, a strong CCW vortex followed by several

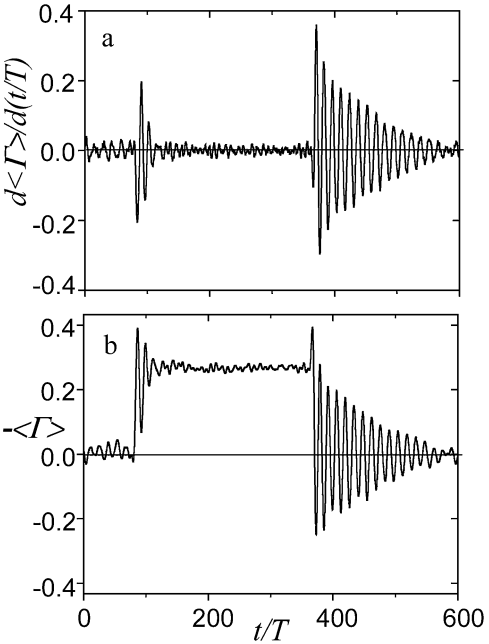

Figure 18 The time response of (*a*) the phase-averaged vorticity flux and (*b*) the incremental change in circulation.

counter-rotating vortices is shed before the wake reaches a limit state that is characterized by a narrower cross section and increased shedding frequency (from 50 to 80 Hz). A similar (but longer) train of counter-rotating vortices is shed following the termination of the modulation where the decrease in the lift force is accompanied by a decrease in circulation.

The dynamic response of the lift force to pulse-modulated actuation is inferred from the time rate of change of the (dimensionless) phase-averaged circulation $d\langle\Gamma\rangle/d(t/T) = \int_{-\infty}^{\infty}\langle U/U_0\rangle \cdot \langle\Omega_z U_0/D\rangle \mathrm{d}(y/D)$, which is estimated from (phase-averaged) cross-stream vorticity flux (not accounting for contributions of the fluctuating components). The incremental change in the circulation with respect to the baseline flow $-\Delta\langle\Gamma\rangle$ is subsequently computed by time integration (see Figure 18). Prior to the onset of modulation, the vorticity flux of the baseline flow exhibits weak oscillations that correspond to passage of counter-rotating wake vortices (Figure 18*a*). Owing to the absence of a clear phase reference prior to the application of actuation (the base flow is not locked to the actuation waveform), the magnitude of the change in the circulation during the passage of successive pairs of counter-rotating wake vortices cannot be estimated from these data.

The onset and termination of the top-hat modulation are accompanied by brief decaying oscillatory bursts of the vorticity flux at the nominal passage frequency of the alternating CW and CCW vortices within the wake. These bursts represent oscillatory flow around the entire cylinder as the circulation is adjusted. A comparison of the bursts following the onset and termination of the modulation indicates there are substantial differences in the characteristic decay times of the circulation transients that are phase locked to the modulation, namely, 2–3 periods and approximately 15 periods of the "natural" shedding frequency, respectively. It appears that the presence of the interaction domain between the jet and the cross flow leads to stronger damping of global flow oscillations around the cylinder that are associated with the changes (increase or decrease) in the overall aerodynamic forces.

4. CONCLUDING REMARKS

Much of the interest in synthetic jets stems from their potential utility for flow control applications, specifically control of the performance of aerodynamic surfaces through fluidic modification of their apparent aerodynamic shape. As shown in Section 3, the interaction domain between a synthetic jet and a cross flow over a solid surface can lead to a local displacement of the cross flow and thereby induce an "apparent" modification of the flow boundary and alter the local pressure and vorticity distributions. Earlier investigations have shown that these attributes may be exploited to modify or control the evolution of wall-bounded and free-shear flows (e.g., flow separation, jet vectoring, vortex flows, etc.) on scales that are one to two orders of magnitude larger than the characteristic length scale of the jets themselves. Furthermore, active modification of the apparent shape of aerodynamic surfaces could enable the tailoring of the pressure gradient on existing aerodynamic surfaces to overcome effects of adverse pressure gradients and local separation, thereby enabling unconventional aerodynamic design approaches that are driven primarily by mission constraints (e.g., payload, stealth, volume, etc.). In that case, the compromised aerodynamic performance of such designs could potentially be augmented by the use of apparent surface modification to maintain acceptable aerodynamic performance.

An important issue in terms of control effectiveness is the characteristic time scale of the actuation. Several investigations of the suppression of flow separation on airfoils, for example, have emphasized actuation frequencies that can couple directly to the instability mechanisms of the separating shear layer in order to effect a Coanda-like reattachment. This approach relies explicitly on the narrowband receptivity of the separating shear layer to a control input that is effective within a limited spatial domain (typically immediately upstream of separation) where the excitation is applied at a frequency that is of the order of the unstable frequency of the base flow such that the excitation period nominally scales with the time of flight over the length of the reattached flow. In contrast, recent work (Smith et al. 1998, Amitay et al. 2001) demonstrated the utility of synthetic jet actuators for suppression of separation at moderate Reynolds numbers

[$O(10^6)$] using actuation frequencies that are at least an order of magnitude higher than the characteristic (e.g., shedding) frequency of the airfoil. This approach emphasizes an actuation frequency that is high enough so that the interaction domain between the actuator and the cross flow is virtually invariant on the global time scale of the flow, and therefore, global effects such as changes in aerodynamic forces are effectively decoupled from the operating frequency of the actuators. At the same time, the broader control bandwidth can also be used to augment the quasi-steady aerodynamic forces by exploiting a prescribed unsteadiness of the separated flow domain using a temporally modulated actuation input to control the rate of vorticity shedding into the wake.

ACKNOWLEDGMENTS

The authors gratefully acknowledge numerous important contributions by A.M. Honohan, B.L. Smith (currently at Los Alamos National Laboratory), and M.A. Trautman (currently at Intel Corporation) during the course of the work and the preparation of the manuscript. This work has been supported in major part by the Air Force Office of Scientific Research. Additional support was provided by NASA Langley Research Center.

LITERATURE CITED

Amitay M, Honohan AM, Trautman M, Glezer A. 1997. Modification of the aerodynamic characteristics of bluff bodies using fluidic actuators. *28th AIAA Fluid Dyn. Conf. 97-2004*, Snowmass, Colo.

Amitay M, Kibens V, Parekh DE, Glezer A. 1999. Flow reattachment dynamics over a thick airfoil controlled by synthetic jet actuators. *37th AIAA Aerosp. Sci. Meet. 99-1001, Reno, Nev.*

Amitay M, Smith BL, Glezer A. 1998. Aerodynamic flow control using synthetic jet technology. *36th AIAA Aerosp. Sci. Meet. 98–0208, Reno, Nev.*

Amitay M, Smith DR, Kibens V, Parekh DE, Glezer A. 2001. Aerodynamic flow control over an unconventional airfoil using synthetic jet actuators. *AIAA J.* 39:361–70

Auerbach D. 1987. Experiments on the trajectory and circulation of the starting vortex. *J. Fluid Mech.* 183:185

Chen FJ, Yao C, Beeler GB, Bryant RG, Fox RL. 2000. Development of synthetic jet actuators for active flow control at NASA Langley. *AIAA Fluids Meet. 2000-2405, Denver, Colo.*

Coe DJ, Allen MG, Smith BL, Glezer A. 1995. Addressable micromachined jet arrays. *Technical Digest: TRANSDUCERS '95.* Stockholm, Sweden

Coe DJ, Allen MG, Trautman M, Glezer A. 1994. Micromachined jets for manipulation of macro flows. *Technical Digest: Solid-State Sensor and Actuator Workshop*, pp. 243–47

Crook A, Sadri AM, Wood NJ. 1999. The development and implementation of synthetic jets for control of separated flow. *AIAA 17th Appl. Aerodyn. Conf. 99-3176, Reno, Nev.*

Crook A, Wood NJ. 2001. Measurements and visualizations of synthetic jets. *AIAA 39th Aerosp. Sci. Meet. 2001-0145, Reno, Nev.*

Davidson BJ, Riley N. 1972. Jets induced by oscillatory motion. *J. Fluid Mech.* 53:287–303

Davis SA, Glezer A. 1999. Mixing control of fuel jets using synthetic jet technology. *AIAA 37th Aerosp. Sci. Meet. 99-0447, Reno, Nev.*

Dhanak MR, Bernardinis B. 1981. The evolution of an elliptic vortex ring. *J. Fluid Mech.* 109:189–216

Didden N. 1979. On the formation of vortex rings: rolling-up and production of circulation. *Z. Angew. Math. Phys.* 30:101–6

Erk PP. 1997. *Separation control on a post-stall airfoil using acoustically generated perturbations*. PhD thesis. Tech. Univ. Berlin, Ger. 159 pp.

Fabris D, Williams DR. 1999. Experimental measurements of cavity and shear layer response to unsteady bleed forcing. *AIAA 37th Aerosp. Sci. Meet. 99-605, Reno, Nev*.

Glezer A. 1988. The formation of vortex rings. *Phys. Fluids* 31:3532–42

Guo D, Kral LD. 2000. Numerical simulation of the interaction of adjacent synthetic jet actuators. *AIAA Fluids 2000 Meet. 2000-2565, Denver, Colo*.

Heskestad G. 1965. Hot-wire measurements in a plane turbulent jet. *ASME J. Appl. Mech.* 32:721–34

Ho CM, Gutmark E. 1987. Vortex induction and mass entrainment in a small-aspect-ratio elliptic jet. *J. Fluid Mech.* 179:383–405

Honohan AM, Amitay M, Glezer A. 2000. Aerodynamic control using synthetic jets. *AIAA Fluids Meet. 2000-2401, Denver, Colo*.

Ingard U, Labate S. 1950. Acoustic circulation effects and the nonlinear impedance of orifices. *J. Acoust. Soc. Am.* 22:211–19

James RD, Jacobs JW, Glezer A. 1996. A round turbulent jet produced by an oscillating diaphragm. *Phys. Fluids* 8:2484–95

Kang E, Breuer KS, Tan CS. 2000. Aerodynamic control using synthetic jets. *AIAA Fluids 2000 Meet. 2000-2232, Denver, Colo*.

Kotsovinos NE, Angelidis PB. 1991. The momentum flux in turbulent submerged jets. *J. Fluid Mech.* 229:453–70

Kovasznay LSG, Fujita H, Lee RL. 1973. Unsteady turbulent puffs. *Adv. Geophys.* 18B: 253–63

Kral LD, Donovan JF, Cain AB, Cary AW. 1997. Numerical simulation of synthetic jet actuators. *28th AIAA Fluid Dyn. Conf. 97-1824, Reno, Nev*.

Lamp AM, Chokani N. 1999. Control of cavity resonance using steady and oscillatory blowing. *AIAA 37th Aerosp. Sci. Meet. 99-0999, Reno, Nev*.

Lebedeva IV. 1980. Experimental study of acoustic streaming in the vicinity of orifices. *Sov. Phys. Acoust.* 26:331–33

Lee CY, Goldstein DB. 2000. Two-dimensional synthetic jet simulation. *AIAA Fluids Meet. 2000-0406, Denver, Colo.*

Lee M, Reynolds WC. 1985. Bifurcating and blooming jets. *AFOSR Tech. Rep. TF-22*

Lighthill J. 1978. Acoustic streaming. *J. Sound Vib.* 61:391–418

Lorkowski T, Rathnasingham R, Breuer KS. 1997. Small-scale forcing of a turbulent boundary layer. *AIAA 28th Fluid Dyn. Conf. 97-1792*

Mallinson SG, Hong G, Reizes JA. 1999. Some characteristics of synthetic jets. *AIAA 30th Fluid Dyn. Conf. 99-3651, Norfolk, VA*

Mallinson SG, Reizes JA, Hong G, Haga H. 2000. The operation and application of synthetic jet actuators. *AIAA Fluids Meet. 2000-2402, Denver, Colo.*

McCormick DC. 2000. Boundary layer separation with directed synthetic jets. *AIAA 38th Aerosp. Sci. Meet. 2000-0519, Reno, Nev*.

Mednikov EP, Novitskii BG. 1975. Experimental study of intense acoustic streaming. *Sov. Phys. Acoust.* 21:152–54

Muller MO, Bernal LP, Miska PK, Washabaugh PD, Chou TKA, et al. 2001. Flow structure and performance of axisymmetric synthetic jets. *AIAA 39th Aerosp. Sci. Meet. 2001-1008, Reno, Nev.*

Muller MO, Bernal LP, Moran RP, Washabaugh PD, Parviz BA, et al. 2000. Thrust performance of micromachined synthetic jets. *AIAA Fluids Meet. 2000-2404*

Palaniswamy S. 2000. *Metacomp technologies.* AVIA Rep.

Perkins CD, Hazen D. 1953. Some recent advances in boundary layer and circulation

control. *4th Anglo-Am. Aeronaut. Conf.*, London, UK

Rediniotis OK, Ko J, Yue X, Kurdila AJ. 1999. Synthetic jets, their reduced order modeling and applications to flow control. *AIAA 37th Aerosp. Sci. Meet. 99-1000, Reno, Nev.*

Riley N, Wibrow MF. 1995. The flow induced by the torsional oscillations of an elliptic cylinder. *J. Fluid Mech.* 290:279–98

Rizzetta DP, Visbal MR, Stanek MJ. 1998. Numerical investigation of synthetic jet flowfields. *29th AIAA Fluid Dyn. Conf. 98-2910, Albuquerque, New Mex.*

Saffman PG. 1981. Dynamics of vorticity. *J. Fluid Mech.* 106:49–58

Schewe G. 1983. On the forced fluctuations acting on a circular cylinder in a cross flow from sub-critical to a trans-critical Reynolds numbers. *J. Fluid Mech.* 133:265–85

Seifert A, Pack LG. 1999. Oscillatory control of separation at high Reynolds numbers. *AIAA J.* 37(9):1062–71

Shih WCL, Wang C, Coles D, Roshko A. 1993. Experiments on flow past rough circular cylinders at large Reynolds numbers. *J. Wind Eng. Ind. Aerodyn.* 49:351–68

Smith BL. 1999. *Synthetic jets and their interaction with adjacent jets*. PhD thesis. Ga. Inst. Technol. 143 pp.

Smith BL, Glezer A. 1994. Vectoring of a high aspect ratio air jet using zero-net-mass-flux control jet. *Bull. Am. Phys. Soc.* 39:1894

Smith BL, Glezer A. 1997. Vectoring and small-scale motions effected in free shear flows using synthetic jet actuators. *AIAA 35th Aerosp. Sci. Meet. 97-0213*

Smith BL, Glezer A. 1998. The formation and evolution of synthetic jets. *Phys. Fluids* 31:2281–97

Smith BL, Trautman MA, Glezer A. 1999. Controlled interactions of adjacent synthetic jets. *AIAA 37th Aerosp. Sci. Meet. 99-0669*

Smith DR, Amitay M, Kibens V, Parekh DE, Glezer A. 1998. Modification of Lifting body aerodynamics using synthetic jet actuators. *36th AIAA Aerosp. Sci. Meet. 98-0209, Reno, Nev.*

Stuart JT. 1966. Double boundary layers in oscillatory viscous flow. *J. Fluid Mech.* 24: 673–87

Williams DR, Acharya M, Bernhardt J, Yang PM. 1991. The mechanism of flow control on a cylinder with the unsteady bleed technique. *AIAA 29th Aerosp. Sci. Meet. 91-0039, Reno, Nev.*

Wiltse JM, Glezer A. 1998. Direct excitation of small-scale motions in free shear flows. *Phys. Fluids* 10(8):2026–36

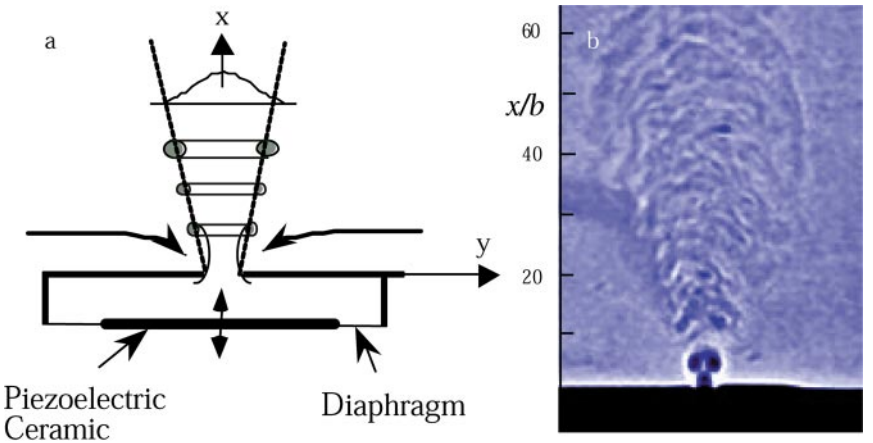

Figure 1 (*a*) Schematic diagram of a synthetic jet actuator and (*b*) Schlieren image of a rectangular synthetic jet. $Re_{l_0} = 18, 124$ ($Re_{U_0} = 383$), $b = 0.5$ mm, and $f =$ 1140 Hz.

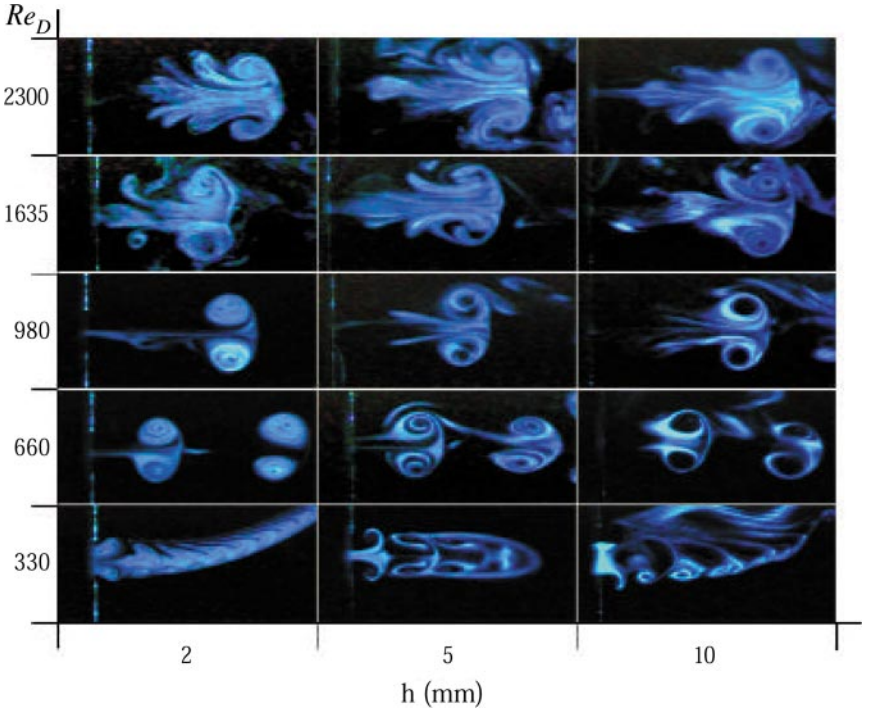

Figure 2 The effects of Re_D and orifice length on the vortices within a synthetic jet (from Crook & Wood 2001). $D = 5$ mm, and $f = 50$ Hz.

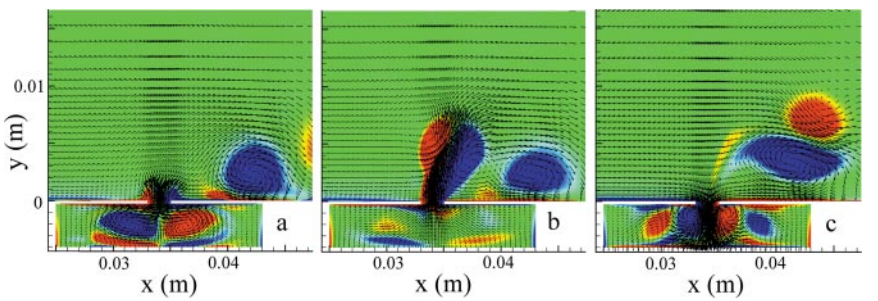

Figure 13 Superimposed velocity vector field and vorticity field at different phases during the actuation cycle (from Palaniswamy 2000).

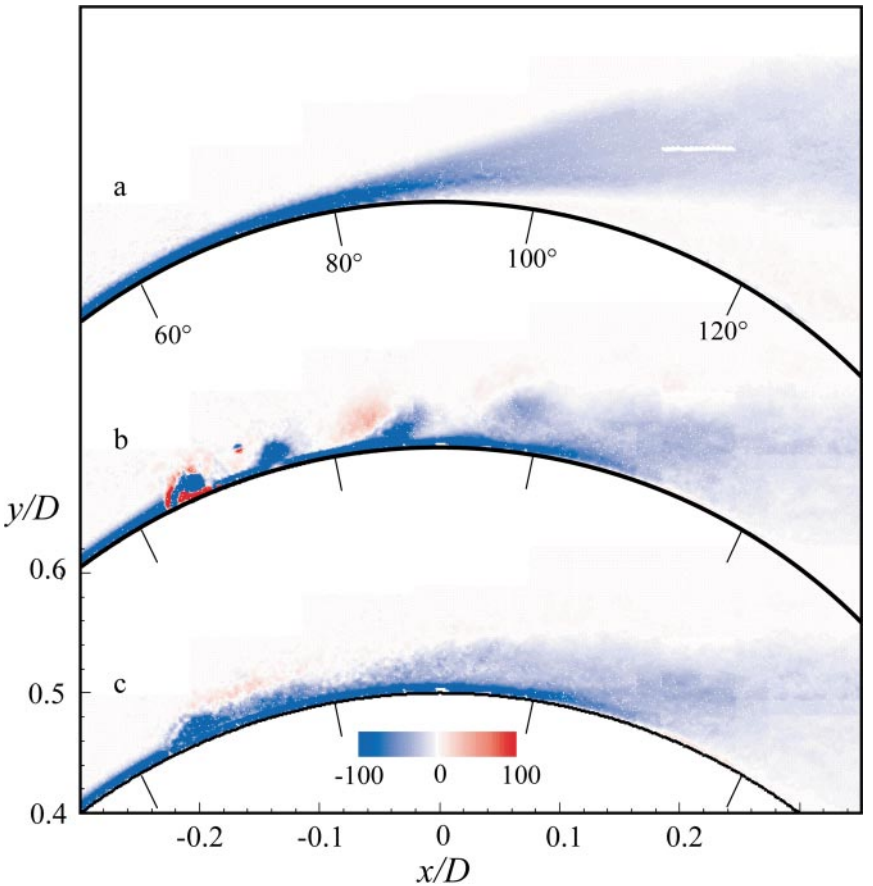

Figure 14 Normalized vorticity. $Re_D = 21{,}500$, $\gamma = 63^0$, $C_\mu = 5.1 \times 10^{-2}$, $\hat{f} = 0.035$. (*a*) baseline; actuated: (*b*) phase locked and (*c*) time averaged.

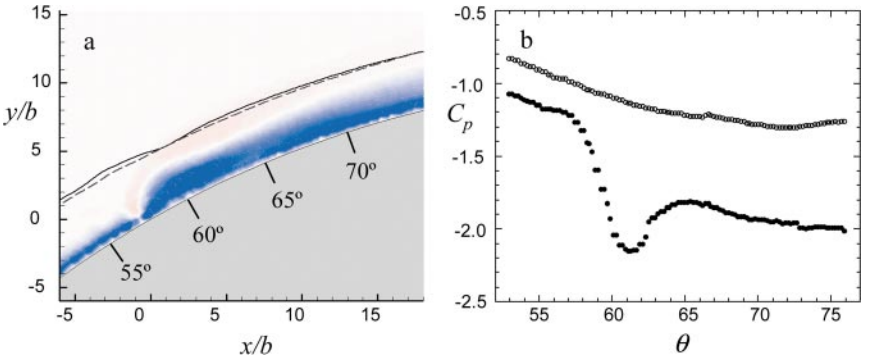

Figure 16 (*a*) Vorticity in interaction domain superimposed with streamlines of the same streamfunction value: (- -) baseline and (—) actuated. (*b*) The pressure coefficient along the streamline: (○) baseline and (●) actuated.

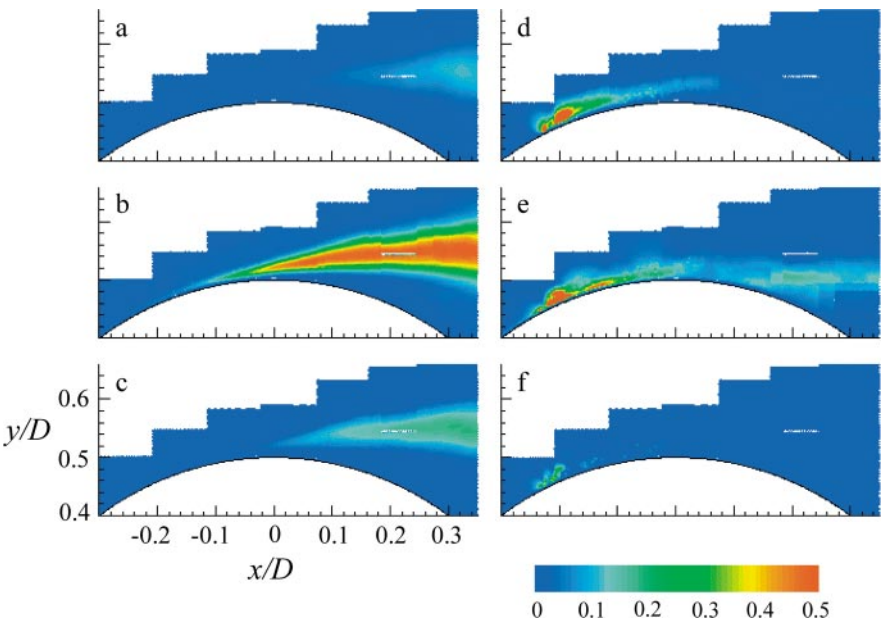

Figure 17 Normalized Reynolds stresses, $Re_D = 21{,}500$. Baseline (*left column*) and actuated (*right column*). $C_\mu = 5.1 \times 10^{-2}$, $\gamma = 63^0$, $\hat{f} = 0.035$. (*a*, *d*) $\overline{u_r' u_r'}/U^2$, (*b*, *e*) $\overline{u_\vartheta' u_\vartheta'}/U^2$, and (*c*, *f*) $\overline{u_r' u_\vartheta'}/U^2$.

Annual Review of Fluid Mechanics
Volume 34, 2002

CONTENTS